

# Record Multiphoton-Absorption Cross-Sections by Dendrimer Organometallation

Peter V. Simpson, Laurance A. Watson, Adam Barlow, Genmiao Wang, Marie P. Cifuentes, Mark G. Humphrey\*

Dedicated to Professor Gerhard Erker on the occasion of his 70th birthday

**Abstract:** We demonstrate large increases in molecular two-photon absorption, the onset of measurable molecular three-photon absorption, and record molecular four-photon absorption in organic  $\pi$ -delocalizable frameworks by incorporation of ligated metal units via organometallic alkynyl linkages. Our resultant ruthenium alkynyl-containing dendrimers exhibit strong multi-photon absorption activity through the biological and telecommunications windows in the near-infrared region. The ligated ruthenium units significantly enhance solubility and introduce fully-reversible redox switchability to the optical properties. Increasing the ruthenium content leads to substantial increases in multiphoton absorption properties without any loss of optical transparency. This significant improvement in multiphoton absorption performance by incorporation of bis(diphosphine)ruthenium alkynyl units into the organic  $\pi$ -framework is maintained when the relevant parameters are scaled by molecular weights or number of delocalizable  $\pi$ -electrons. The four-photon absorption cross-section of the most metal-rich dendrimer is an order of magnitude greater than the previous record value.

The multiphoton-absorption (MPA) properties of molecular materials are of rapidly increasing interest due to the demonstrated or potential use of MPA-active materials in frequency upconversion lasing, imaging, and microscopy, optical power limiting, microfabrication, data storage and processing, and various biological and medical applications.<sup>[1]</sup> This strong current focus, and the consequent need to maximize the relevant MPA coefficients, has prompted a push to develop structure-MPA property relationships (particularly for two-photon absorption, 2PA) to facilitate the design of efficient MPA materials. For example, while early studies identified the efficiency of dipolar molecules, subsequent research revealed that quadrupolar and octupolar species could be similarly or more efficient while possessing optical transparency advantages.<sup>[2-5]</sup> In parallel, the materials processing advantages that accrue in proceeding from small molecules to (polydisperse) polymers and (monodisperse) dendrimers were noted.

The vast majority of studies of MPA-active molecular materials have thus far focused on purely organic species. However, transition metal-containing molecules (with a diversity of possible metals and their multiple accessible oxidation states, ligands, and coordination geometries)<sup>[6-9]</sup> may provide versatile means to

optimize MPA properties. Comparisons of the 2PA efficiencies of analogous organic molecules and transition metal complexes are sparse, while comparisons of higher-order MPA effects such as three-photon absorption (3PA) are non-existent, but the very limited results thus far employing a range of scaling factors [molecular weight, molecular volume, effective number of delocalizable electrons (in an approach based on fundamental quantum principles), and cost of production] suggest that the MPA efficiencies of inorganic complexes are potentially superior to those of organic compounds.<sup>[10-12]</sup> Despite this tantalizing outcome, no reports thus far have examined and directly compared the MPA efficiencies of strictly analogous organic and transition metal-containing dendrimers to shed light on this key concern. We report herein the syntheses of three structurally-related first-generation aryleneethynylene-based organic dendrimers with varying levels of metal content, together with broad spectral range (500-1700 nm) femtosecond Z-scan studies exploring their nonlinear absorption properties; we find that increasing metal content leads to dramatic increases in (i) 2PA in the technologically important therapeutic window, at wavelengths corresponding to maximum transparency of biological material such as tissue, and (ii) 3PA in the technologically important telecommunications window, at wavelengths corresponding to maximum transparency of silica, as well as (iii) the onset of measurable 4PA at longer wavelengths in the near infrared (NIR) region.

The dendrimers employed in the present study are depicted in **Figure 1**; complete synthetic details are provided in the Supporting Information. All three dendrimers feature  $\pi$ -delocalizable oligo(phenyleneethynylene) (OPE) frameworks; OPEs and related oligo(phenylenevinylene)s have been amongst the most popular  $\pi$ -delocalizable frameworks in organic 2PA molecular materials design.<sup>[1]</sup> 4-Methoxy-3,5-di(*tert*-butyl)phenyl units were installed at the periphery of all three dendrimers to ensure sufficient solubility of the purely organic dendrimer **Ru0** for the nonlinear optical (NLO) studies [the bis(diphosphine)ruthenium units afford sufficient solubility for the organometallic dendrimers **Ru3** and **Ru9**, as has also been shown in studies with related species;<sup>[13-16]</sup> nevertheless, **Ru3** and **Ru9** have been identically peripherally functionalized for consistency and thereby comparability]. The ligated ruthenium units were chosen for several reasons: (i) the 18-valence-electron count at the ruthenium centers has been shown to be advantageous for maximizing NLO coefficients in comparison with metal centers with lower valence electron counts;<sup>[17]</sup> (ii) bis(diphosphine)ruthenium centers undergo facile oxidation accompanied by strong changes in linear and nonlinear optical properties, adding important functionality;<sup>[18]</sup> and (iii) the dichloro precursor to complexes with this specific coordination

[\*] Organometallic Complexes for Nonlinear Optics. 55.

Dr. P. V. Simpson, L. A. Watson, Dr A. Barlow, Dr G. Wang,  
Assoc. Prof. M. P. Cifuentes, Prof. M. G. Humphrey  
Research School of Chemistry,  
Australian National University, Canberra, ACT 2601, Australia  
E-mail: Mark.Humphrey@anu.edu.au

## COMMUNICATION

environment permits facile stepwise replacement of the chloro ligands and thereby formation of the axially-coordinated unsymmetrical bis(alkynyl) coordination environment<sup>[19]</sup> needed for efficient dendrimer synthesis.<sup>[20]</sup>

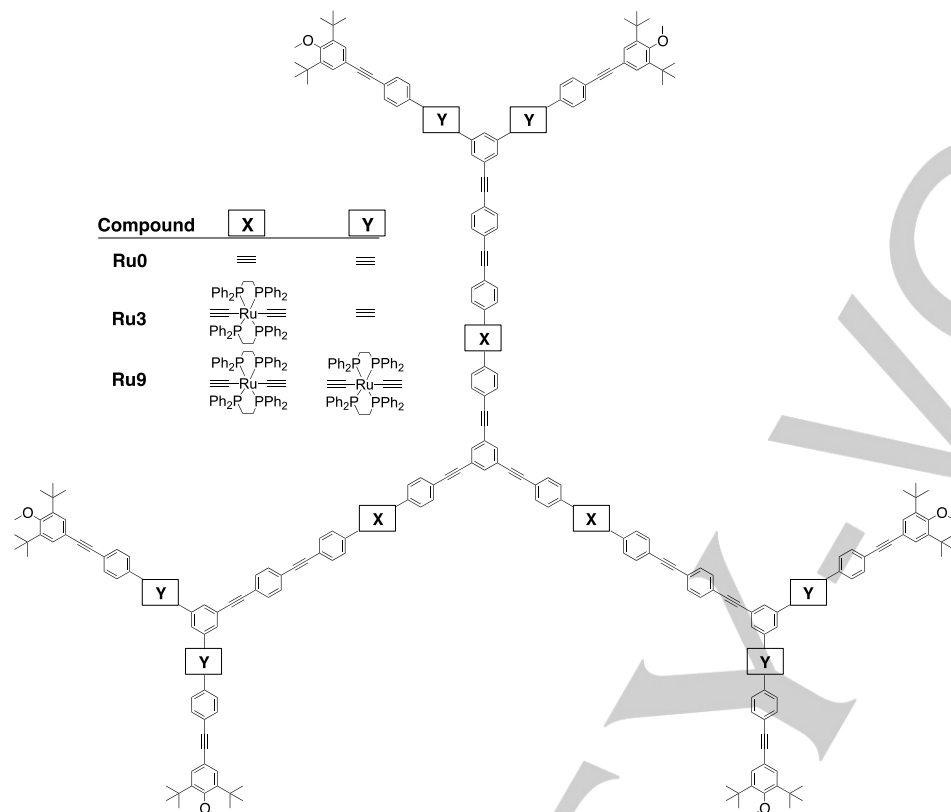


**Figure 1.** Molecular structures of **Ru0**, **Ru3**, and **Ru9**.

The new compounds were characterized by the conventional spectroscopies (Supporting Information). The <sup>31</sup>P NMR spectra of **Ru3** (Figure S16) and **Ru9** (Figure S23) feature singlets, consistent with *trans*-disposed bis(diphenylphosphino)ethane (dppe) ligands;<sup>[20]</sup> the former possesses one resonance (54.10 ppm) corresponding to the “inner” Ru( $\kappa^2$ -dppe)<sub>2</sub> units, while the latter shows two resonances (54.32, 54.11 ppm, ratio 2:1) corresponding to the “outer” and “inner” Ru( $\kappa^2$ -dppe)<sub>2</sub> groups, respectively. The linear optical spectrum of **Ru0** (Figure S24) features several overlapping bands in the range 330–370 nm assigned to transitions in the OPE framework  $\pi$ -manifold.<sup>[21]</sup> Progression to **Ru3** results in the appearance of a low-energy band at ca. 430 nm corresponding to (a) MLCT transition(s),<sup>[15,18]</sup> which persists on proceeding to **Ru9**, and which is accompanied by the appearance of a strong band at ca. 380 nm corresponding to (a) further MLCT transition(s); thus, MLCT occurs at a lower energy in the interior dendrimer sites than at the periphery (Figure S24). **Ru0** exhibits fluorescence when excited at 350 nm (Figure S25); this luminescence is quenched upon ruthenium incorporation, on proceeding from **Ru0** to **Ru3** and **Ru9**. The cyclic voltammogram (CV) of **Ru0** is featureless across the scan range -1.5 to +1.5 V; in contrast, the CVs of **Ru3** and **Ru9** each

exhibit one reversible metal-centered oxidation process at 0.57 V (Table S1). UV-vis-NIR spectroelectrochemical studies of **Ru3** (Figure S26) and **Ru9** (Figure S27) with applied potentials of +0.9 V reveal the appearance of low-energy bands at 1250 nm

corresponding to LMCT transitions in the oxidized species **Ru3**<sup>3+</sup> and **Ru9**<sup>9+</sup>, by analogy with related dendrimers.<sup>[15]</sup> Thus, incorporation of the ligated ruthenium centers results in the loss of fluorescence, but adds other beneficial functionality to the dendrimer: strong charge-transfer bands in the optical spectra, reversible redox activity accompanied by strong optical changes, and enhanced solubility.

The nonlinear absorption and nonlinear refraction properties of **Ru0** (Figure S29), **Ru3** (Figure S31), and **Ru9** (Figure S33) were assessed by the Z-scan technique over the spectral range 500–1700 nm, and employing ca. 130 femtosecond pulses to minimize contributions to nonlinear absorption from excited state-absorption (ESA). Closed- and open-aperture experiments were undertaken, affording simultaneous evaluation of the spectral dependencies of the absorptive and refractive components of the hyperpolarizability. For all three

dendrimers, the real part of the nonlinearity  $\gamma_{\text{real}}$  is negative or zero over the spectral range surveyed, with negative maximal values of  $\gamma_{\text{real}}$  at approximately coincident wavelengths to positive maximal values of  $\gamma_{\text{imag}}$ , and therefore consistent with the expected dependence of  $\gamma_{\text{real}}$  on all nonlinear absorption processes through a nonlinear Kramers-Kronig relationship.<sup>[22]</sup> The absorptive nonlinearities replotted as the effective two-photon absorption cross-sections are presented in Figures S28 (**Ru0**), S30 (**Ru3**), and S32 (**Ru9**), together with the linear optical absorption spectra plotted at twice, three times, and four times the wavelength. All three compounds show maxima at ca. 600 nm; in the case of **Ru0** (Table 1), this has been confirmed as 2PA in nature from examination of the intensity dependence of the open-aperture fs Z-scan trace (Figure S34). **Ru0** has effectively no nonlinear absorption activity at wavelengths longer than 800 nm (Figure S35); in contrast, **Ru3** and **Ru9** exhibit significant nonlinear absorption at longer wavelengths. Both **Ru3** and **Ru9** possess local MPA maxima in the region 760–780 nm. The near coincidence of these MPA maxima with twice the wavelengths of linear optical absorption maxima is suggestive of two-photon absorption (Figures 2 and 3). This MPA behavior at 760–780 nm has been confirmed as 2PA in nature (Figure S36), and with a significant increase in 2PA cross-section on increasing metallation (**Ru3**: 4400 GM; **Ru9**: 17000 GM) (Table 1). The ruthenium-containing dendrimers also exhibit local MPA maxima in the spectral region 1100–1200 nm that are at wavelengths similar to three-times the wavelength of the linear optical

## COMMUNICATION

absorption maxima (Figures 2 and 3), the MPA behavior being confirmed as 3PA in nature from comparison of the open-aperture Z-scan traces to theoretical fits corresponding to 2PA and 3PA (Figures S37 and S38); the 3PA cross-section increases substantially on increasing ruthenium content (**Ru3**:  $3500 \times 10^{-80} \text{ cm}^6 \text{ s}^{-2}$ ; **Ru9**:  $10000 \times 10^{-80} \text{ cm}^6 \text{ s}^{-2}$ ) (Table 1). Finally, the more heavily ruthenated dendrimer **Ru9** is unique in exhibiting significant MPA behavior at ca. 1600 nm (Figure 3), confirmed as 4PA in character (Figure S39), and substantial in magnitude ( $2100 \times 10^{-110} \text{ cm}^8 \text{ s}^{-3}$  at 1600 nm) (Table 1).

**Table 1.** Linear optical absorption and nonlinear optical absorption cross-section maxima for dendrimers **Ru0**, **Ru3**, and **Ru9**.<sup>a)</sup>

Complex	$\lambda_{1,\text{max}}^{[\text{b}]}$ [e] <sup>[c]</sup>	$\lambda_{2,\text{max}}^{[\text{b}]}$ [e] <sup>[c]</sup>	$\sigma_2^{[\text{d}]}$ ( $\lambda_{\text{max}}^{[\text{b}]}$ )	$\sigma_3^{[\text{e}]}$ ( $\lambda_{\text{max}}^{[\text{b}]}$ )	$\sigma_4^{[\text{f}]}$ (1 m)
<b>Ru0</b>	356 [54]	-	1200 (600) 60 (760)	0	0
<b>Ru3</b>	333 [45]	424 [18]	4400 (760)	3500 (1100)	0
<b>Ru9</b>	311 [40]	390 [59]	17000 (780)	10000 (1200)	2100

<sup>[a]</sup>  $\text{CH}_2\text{Cl}_2$ , <sup>[b]</sup> nm, <sup>[c]</sup>  $10^4 \text{ M}^{-1} \text{ cm}^{-1}$ , <sup>[d]</sup>  $\text{GM} = 10^{-50} \text{ cm}^4 \text{ s}$ , <sup>[e]</sup>  $10^{-80} \text{ cm}^6 \text{ s}^2$ , <sup>[f]</sup>  $10^{-110} \text{ cm}^8 \text{ s}^3$ .

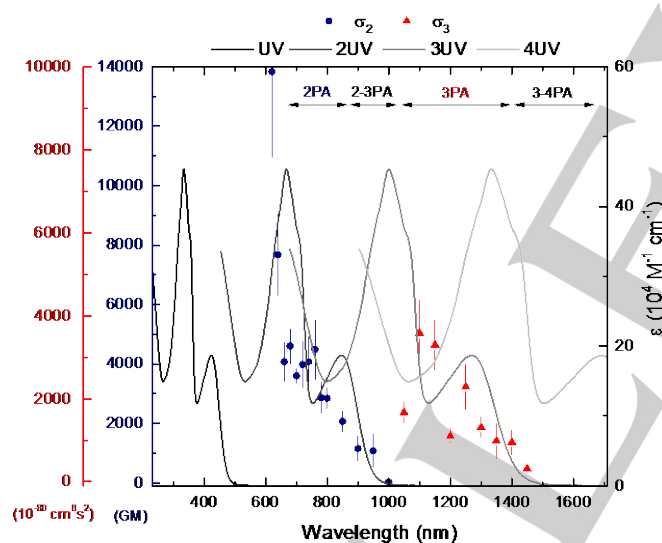


**Figure 2.** Plot of  $\sigma_2$  (blue) and  $\sigma_3$  (red) for **Ru3** overlaid on the UV-visible spectrum (black), and including plots of the UV-visible spectrum as a function of twice (dark gray), three-times (gray) and four-times (light gray) the wavelength.

Given the broad range of molecular materials that have attracted attention for putative NLO applications, the assessment of their comparative NLO efficiency is of significant interest. The NLO efficiency of organometallics may exceed that of organic molecules when the data are scaled in a variety of ways (e.g. considering molecular volume, the cost of production or the number of delocalizable electrons contributing to the NLO performance),<sup>[10-12]</sup> but the limited precedents involve structurally

diverse compounds. The present study provides the first opportunity to evaluate comparative NLO merit for systematically varied rather than disparate molecules, the ruthenated dendrimers differing from **Ru0** by incorporation of three (**Ru3**) or nine (**Ru9**) *trans*-[Ru(C≡C)-(dppe)<sub>2</sub>] units into an otherwise invariant organic  $\pi$ -delocalizable skeleton. These molecular modifications are accompanied by key differences in the linear optical absorption spectra and enhancement of the MPA behavior, even when scaled by molecular weight or number of effective  $\pi$ -delocalizable electrons<sup>[11a]</sup> (Table 2). Thus, the scaled maximal  $\sigma_2$  values in the 760-780 nm region increase dramatically on metallation, a significant increase being maintained on broadening the **Ru0** window to include the  $\sigma_2$  maximum at 600 nm (an approximate doubling of  $\sigma_{2,\text{max}}/M$  is seen on proceeding from **Ru0** to **Ru3**, and then again to **Ru9**, while the increase in  $\sigma_{2,\text{max}}/N_{\text{eff}}^2$  is even more significant). A similar significant increase is seen in the 3PA region of the MPA spectra; **Ru0** displays no measurable activity, and the scaled  $\sigma_3$  data increase substantially on proceeding from **Ru3** to **Ru9**. Increasing levels of metallation "switches on" measurable 4PA efficiency; while **Ru0** and **Ru3** do not exhibit detectable 4PA activity, **Ru9** shows a large 4PA cross-section at 1600 nm (Table 2).

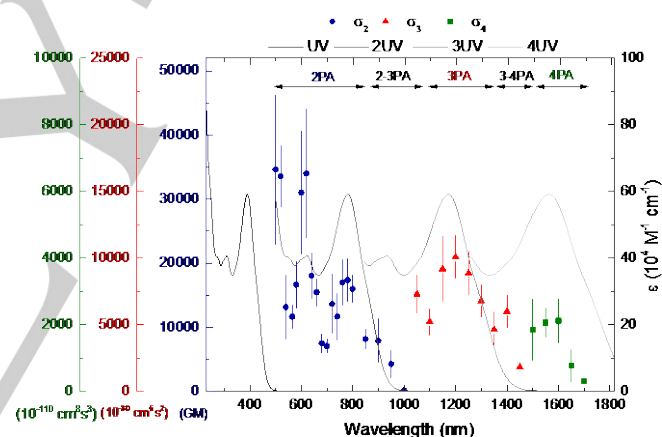


**Figure 3.** Plot of  $\sigma_2$  (blue),  $\sigma_3$  (red) and  $\sigma_4$  (green) for **Ru9** overlaid on the UV-visible spectrum (black), and including plots of the UV-visible spectrum as a function of twice (dark gray), three-times (gray) and four-times (light gray) the wavelength.

**Table 2.** Comparison of the molecular weight- and effective-number-of- $\pi$ -electrons-scaled NLO parameters at local maxima for **Ru0**, **Ru3**, and **Ru9**.<sup>[a]</sup>

Complex	$\sigma_2/M$ , ( $\lambda_{\text{max}}^{[\text{c}]}$ )	$\sigma_2/N_{\text{eff}}^2$ [b]	$\sigma_3/M$ , ( $\lambda_{\text{max}}^{[\text{c}]}$ )	$\sigma_3/N_{\text{eff}}^3$ [d]	$\sigma_4/M$ , ( $\lambda_{\text{max}}^{[\text{c}]}$ )	$\sigma_4/N_{\text{eff}}^4$ [e]
<b>Ru0</b>	0.35, 0.24 (600) 0.02, 0.012 (760)		0, 0		0, 0	
<b>Ru3</b>	0.72, 1.23 (760)		0.57, (1150)	0.016	0, 0	
<b>Ru9</b>	1.46, 5.21 (780)		0.86, (1200)	0.054	0.18, (1600)	0.00020

<sup>[a]</sup> CH<sub>2</sub>Cl<sub>2</sub> solvent, N<sub>eff</sub><sup>2</sup> = 5016 (**Ru0**), 3576 (**Ru3**), 3264 (**Ru9**), <sup>[b]</sup> GM mol g<sup>-1</sup>, GM, 1 GM = 10<sup>-50</sup> cm<sup>4</sup> s, <sup>[c]</sup> nm, <sup>[d]</sup> 10<sup>-80</sup> cm<sup>6</sup> s<sup>2</sup> mol g<sup>-1</sup>, 10<sup>-80</sup> cm<sup>6</sup> s<sup>2</sup>, <sup>[e]</sup> 10<sup>-110</sup> cm<sup>8</sup> s<sup>3</sup> mol g<sup>-1</sup>, 10<sup>-110</sup> cm<sup>8</sup> s<sup>3</sup>.

The maximal 3PA and 4PA cross-sections of the most heavily metallated dendrimer **Ru9** are very large in an absolute sense for data acquired under fs conditions (Table S1). Excluding mesoscopic species such as synuclein fibrils<sup>[23]</sup> and semiconductor nanorods,<sup>[24]</sup> comparable 3PA activity for molecules has only been seen with donor- $\pi$ -bridge-donor ladder-type oligo(phenylene)s composed of linear fused 9,9-di(4-decylphenyl)fluorenes ( $\sigma_{3,\max}$  2720 x 10<sup>-80</sup> cm<sup>6</sup> s<sup>2</sup>, <sup>[25]</sup> N<sub>eff</sub><sup>2</sup> 12724,  $\sigma_{3,\max}/N_{\text{eff}}^3$  0.0019 x 10<sup>-80</sup> cm<sup>6</sup> s<sup>2</sup>). Reports of 4PA activity are comparatively scarce;<sup>[1,26]</sup> to the best of our knowledge, **Ru9** possesses the largest 4PA cross-section measured under fs conditions thus far, ca. twenty five times larger than that of the highly efficient 7-benzothiazol-2-yl-9-didecylfluoren-2-yl)diphenylamine ( $\sigma_{4,\max}$  81 x 10<sup>-110</sup> cm<sup>8</sup> s<sup>3</sup>)<sup>[26]</sup> and with similar effective  $\pi$ -electron-scaled 4PA efficiency to that of the organic (N<sub>eff</sub><sup>2</sup> 472,  $\sigma_{4,\max}/N_{\text{eff}}^4$  0.00036 x 10<sup>-110</sup> cm<sup>8</sup> s<sup>3</sup>), and possesses a 4PA cross-section an order of magnitude larger than that reported for semiconductor quantum dots.<sup>[27]</sup>

In conclusion, the present study has demonstrated the advantages of an "organometallation" approach to NLO molecular materials, the benefits including additional functionality (reversible redox capability, enhanced solubility) and greatly increased nonlinear absorption. The significant performance increase noted upon incorporation of ligated metal centers into a dendritic framework has been shown both for experimental data and for data scaled by molecular weight. Progression from the triruthenium to the nonaruthenium dendrimer is achieved with no loss in optical transparency. The absolute maximal values of both the three- and four-photon absorption cross-sections of the most ruthenated dendrimer are exceptionally large, highlighting the NLO efficiency of this molecular composition.

## Experimental Section

Detailed experimental procedures for the synthesis of **Ru0**, **Ru3**, and **Ru9** and their precursors, characterization data, and the nonlinear optical studies are reported in the Supporting Information.

## Supporting Information

Supporting Information is available from the Wiley Online Library or from the author.

## Acknowledgements

We thank the Australian Research Council (Discovery Grant to M.G.H., ARC Australian Research Fellowship to M.P.C.) for financial support. Supporting Information is available online from Wiley InterScience or from the authors.

**Keywords:** Dendrimers, Nonlinear Optics, Photonics, Optically Active Materials

- [1] G. S. He, L.-S. Tan, Q. Zheng, P. N. Prasad, *Chem. Rev.* **2008**, *108*, 1245.
- [2] M. Albota, D. Beljonne, J. L. Bredas, J. E. Ehrlich, J. Y. Fu, A. A. Heikal, S. E. Hess, T. Kogej, M. D. Levin, S. R. Marder, D. McCord-Maughon, J. W. Perry, H. Rockel, M. Rumi, G. Subramaniam, W. W. Webb, X. L. Wu, C. Xu, *Science* **1998**, *281*, 1653.
- [3] B. A. Reinhardt, L. L. Brott, S. J. Clarson, A. G. Dillard, J. C. Bhatt, R. Kannan, L. Yuan, G. S. He, P. N. Prasad, *Chem. Mater.* **1998**, *10*, 1863.
- [4] M. P. Joshi, J. Swiatkiewicz, F. Xu, P. N. Prasad, B. A. Reinhardt, R. Kannan, *Opt. Lett.* **1998**, *23*, 1742.
- [5] B. R. Cho, K. H. Son, S. H. Lee, Y.-S. Song, Y.-K. Lee, S.-J. Jeon, J. H. Choi, H. Lee, M. J. Cho, *J. Am. Chem. Soc.* **2001**, *123*, 10039.
- [6] B. J. Coe, in *Comprehensive Coordination Chemistry II*, J. A. McCleverty, T. J. Meyer, Eds, Elsevier: Oxford, **2004**; Vol. 9, pp 621-687.
- [7] M. E. Thompson, P. E. Djurovich, S. Barlow, S. R. Marder, in *Comprehensive Organometallic Chemistry III*, R. H. Crabtree, D. M. P. Mingos, Eds, Elsevier: Oxford, **2007**; Vol. 12, pp 101-194.
- [8] J. P. Morrall, G. T. Dalton, M. G. Humphrey, M. Samoc, *Adv. Organomet. Chem.* **2008**, *55*, 61.
- [9] M.G. Humphrey, T. Schwich, P.J. West, M.P. Cifuentes, M. Samoc, in *Comprehensive Inorganic Chemistry II*, J. Reedijk, K. Poeppelmeier, Eds, Elsevier: Oxford, **2013**; Vol. 8, pp 781-835.
- [10] R. L. Roberts, T. Schwich, T. C. Corkery, M. P. Cifuentes, K. A. Green, J. D. Farmer, P. J. Low, T. B. Marder, M. Samoc, M. G. Humphrey, *Adv. Mater.* **2009**, *21*, 2318.
- [11] a) M. G. Kuzyk, *J. Chem. Phys.* **2003**, *119*, 8327. b) J. Pérez-Moreno, M. G. Kuzyk, *J. Chem. Phys.* **2005**, *123*, 194101. c) J. Pérez-Moreno, M. G. Kuzyk, *Adv. Mater.* **2011**, *23*, 1428. d) M. G. Kuzyk, J. Pérez-Moreno, S. Shafel, *Phys. Rep.* **2013**, *529*, 297.
- [12] T. Schwich, M. P. Cifuentes, P. A. Gugger, M. Samoc, M. G. Humphrey, *Adv. Mater.* **2011**, *23*, 1433.
- [13] A. M. McDonagh, M. G. Humphrey, M. Samoc, B. Luther-Davies, S. Houbrechts, T. Wada, H. Sasabe, A. Persoons, *J. Am. Chem. Soc.* **1999**, *121*, 1405.
- [14] C. E. Powell, J. P. Morrall, S. A. Ward, M. P. Cifuentes, E. G. A. Notaras, M. Samoc, M. G. Humphrey, *J. Am. Chem. Soc.* **2004**, *126*, 12234.
- [15] M. P. Cifuentes, C. E. Powell, J. P. Morrall, A. M. McDonagh, N. T. Lucas, M. G. Humphrey, M. Samoc, S. Houbrechts, I. Asselberghs, K. Clays, A. Persoons, T. Isoshima, *J. Am. Chem. Soc.* **2006**, *128*, 10819.
- [16] M. Samoc, J. P. Morrall, G. T. Dalton, M. P. Cifuentes, M. G. Humphrey, *Angew. Chem. Int. Ed.* **2007**, *46*, 731.
- [17] I. R. Whittall, M. P. Cifuentes, M. G. Humphrey, M. Samoc, B. Luther-Davies, S. Houbrechts, A. Persoons, G. A. Heath, D. Bogsanyi, *Organometallics* **1997**, *16*, 2631.
- [18] C. E. Powell, M. P. Cifuentes, J. P. L. Morrall, R. Stranger, M. G. Humphrey, M. Samoc, B. Luther-Davies, G. A. Heath, *J. Am. Chem. Soc.* **2003**, *125*, 602.
- [19] D. Touchard, P. Haquette, N. Pirio, L. Toupet, P. H. Dixneuf, *Organometallics* **1993**, *12*, 3132.
- [20] A. M. McDonagh, C. E. Powell, J. P. Morrall, M. P. Cifuentes, M. G. Humphrey, *Organometallics* **2003**, *22*, 1402.
- [21] U. H. F. Bunz, *Chem. Rev.* **2000**, *100*, 1605.
- [22] M. Sheikh-Bahae, D. J. Hagan, E. W. van Stryland, *Phys. Rev. Lett.* **1990**, *65*, 96.
- [23] P. Hanczyc, M. Samoc, B. Norden, *Nature Photon.* **2013**, *7*, 969.
- [24] G. Xing, S. Chakraborty, S. W. Ngiam, Y. Chan, T. C. Sum, *J. Phys. Chem. C* **2011**, *115*, 17711.
- [25] H. H. Fan, L. Guo, K. F. Li, M. S. Wong, K. W. Cheah, *J. Am. Chem. Soc.* **2012**, *134*, 7297.
- [26] F. E. Hernandez, K. D. Belfield, I. Cohanoschi, M. Balu, K. J. Schafer, *Appl. Opt.* **2004**, *43*, 5394.



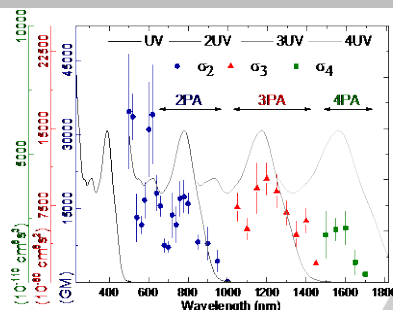
- [27] J. Szeremeta, M. Nyk, D. Wawrzynczyk, M. Samoc, *Nanoscale* **2013**, *5*, 2388.

WILEY-VCH

---

## COMMUNICATION

Incorporation of ligated metal units into a dendritic structure leads to a significant increase in two-photon absorption cross-section scaled by molecular weight or number of delocalizable  $\pi$ -electrons at biologically-important wavelengths, and the appearance of large three- and record four-photon absorption cross-sections in the telecommunications region.



Peter V. Simpson, Laurance A. Watson, Adam Barlow, Genmiao Wang, Marie P. Cifuentes, Mark G. Humphrey\*

Page No. – Page No.

Record Multiphoton-Absorption Cross-Sections by Dendrimer Organometallation